Induction Motor Stator Current AM-FM Model and Demodulation Analysis for Planetary Gearbox Fault Diagnosis

Zhipeng Feng, *Member, IEEE*, Xiaowang Chen, and Ming J. Zuo, *Senior Member, IEEE*

***Abstract*—Induction motor-planetary gearbox drivetrains are widely used for industrial productions, including machine tools in manufacturing systems. For fault diagnosis of planetary gearboxes in such electromechanical systems, motor current signal analysis provides an effective alternative approach, because motor current signals have easier accessibility and are free from time-varying transfer path effects. Planetary gearbox faults generate load torque oscillations, leading to both amplitude modulation and frequency modulation (AM-FM) effects on induction motor current signals. To thoroughly understand gear fault features in current signals, an AM-FM current signal model is derived through mechanical–magnetic–electric interaction analysis, explicit equation of Fourier spectrum is derived, and sidebands characteristics are summarized. To avoid an intricate sideband analysis, amplitude and frequency demodulation analyses are proposed, explicit equations of corresponding demodulated spectra are derived, and gear fault features are summarized. The theoretical derivations are validated through lab experiments. Localized fault on the sun, planet, and ring gears are all successfully diagnosed using the proposed method.**

***Index Terms*—Current signature, fault diagnosis, induction motor, modulation, planetary gearbox.**

Nomenclature

ω_{ps}, ω_g	Power supply and gear fault frequency.
T_m, T_l, T_g	Motor, load, and fault torques.
ω_r, θ_r	Rotor speed and angle.
F_s, F_r, F	Stator, rotor, and total magnetomotive forces.
B_s, B_r, B	Stator, rotor, and total air-gap flux densities.
Φ_s, Φ_r, Φ	Stator, rotor, and total air-gap fluxes.
p, J	Pole pair number and rotary inertia.
V, R_s, I	Stator voltage, resistance, and current.
I_s, I_r	Stator resistant and active current amplitude.
φ	Initial phase.
$J(\cdot), \delta(\cdot)$	Bessel and Dirac delta functions.

Manuscript received April 21, 2018; revised August 8, 2018; accepted September 21, 2018. Date of publication October 12, 2018; date of current version April 3, 2019. This work was supported in part by the National Natural Science Foundation of China (51875034), in part by the Future Energy Systems under Canada First Research Excellent Fund (FES-T14-P02), and in part by the Natural Sciences and Engineering Research Council of Canada under Grant #RGPIN-2015-04897. Paper no. TII-18-0917. *(Corresponding author: Ming J. Zuo.)*

Z. Feng and X. Chen are with the School of Mechanical Engineering, University of Science and Technology Beijing, Beijing 100083, China (e-mail: fengzp@ustb.edu.cn; xiaowang.chen@live.com).

M. J. Zuo is with the Department of Mechanical Engineering, University of Alberta, Edmonton, AB T6G 1H9, Canada (e-mail: ming.zuo@ualberta.ca).

Color versions of one or more of the figures in this paper are available online at http://ieeexplore.ieee.org.

Digital Object Identifier 10.1109/TII.2018.2875447

I. Introduction

PLANETARY gearboxes have unique merits of large transmission ratio and high load capacity in a compact package, and, therefore, are widely used for power transmission in many electromechanical systems, including machine tools in manufacturing industries [1]–[3]. Once a fault occurs to planetary gearboxes, it will result in transmission deficiency and even shutdown of entire system. Hence, planetary gearbox fault diagnosis becomes more and more attractive in electromechanical system diagnostics community.

To date, researchers have made important contributions to planetary gearbox fault diagnosis. To name a few, for example, Chaari *et al.* [4], [5] modeled the dynamic behavior of planetary gearbox under distributed fault and nonstationary operating conditions. Lei *et al.* [6] presented an adaptive stochastic resonance method to suppress noise interference, and extracted weak gear fault feature of a planetary gearbox. Yoon *et al.* [7] developed a spectral averaging method via enveloping and Welch's spectral averaging for planetary gearbox fault diagnosis. Feng *et al.* [8], [9] derived explicit equations for gear fault frequency calculation, summarized the spectral characteristics of vibration signals, and proposed amplitude and frequency demodulation analyses methods for planetary gearbox fault diagnosis. However, all these works focus on vibration signal analysis. In practice, vibration signals are usually collected from vibration sensors fixed on gearbox casing. In this situation, planetary gearboxes feature high vibration complexity because of their intricate structure and involute kinematics, particularly the planet gear revolution around the sun gear and the resultant time-varying gear mesh location relative to vibration sensors. This leads to difficulty in planetary gearbox fault diagnosis via vibration signal analysis.

Electric machine current signature analysis provides a promising alternative approach to planetary gearbox fault diagnosis. In most industrial applications, for example, the spindle in machine tools, planetary gearboxes are usually connected with electric machines to transmit power. Gear faults generate torque

oscillations, and further lead to changes in electric machine currents because of mechanical–magnetic–electric interactions. Therefore, gear faults are manifested by electric machine current signatures, and are detectable through current signal analysis. Moreover, current signature analysis outperforms vibration-based methods for planetary gearbox fault diagnosis, because of their unique merits: 1) easier accessibility. Stator current signals can be collected anywhere from power supply wires connecting to an electric machine, and, therefore, they are free from sensor placement issue [10]–[13]; and 2) a nature free of the extra amplitude modulation (AM) effect due to time-varying propagation paths. Planetary gearboxes are isotropic circumferentially, and, therefore, stator current signatures due to gear fault torsional oscillations do not involve time variability of transfer paths. As such, stator current signals feature simple frequency structures and can exhibit fault signature more effectively.

Recently, gear fault effects on current signatures have been investigated through mechanical—magnetic–electric modeling of electric machine-planetary gearbox system. Zhang *et al.* [14] set up a planetary gearbox-load generator model to study gear fault symptoms in current signals, and utilized a resonance residual technique to extract fault features. Ottewill *et al.* [15] studied epicyclic gearbox fault effects on current signals based on a mathematical model of drive motor-epicyclic gearbox, and detected gear tooth profile errors via a synchronous averaging technique. These works explain the interaction between gear faults and electric machine currents, but a thorough understanding of planetary gearbox fault current signals and an explicit summary on gear fault signatures are still in demand.

In order for a thorough explanation on manifestation of gear faults in current signals and thereby development of effective signal analysis methods, an analytic model of current signals from a signal processing aspect is necessary. Moreover, an explicit derivation of gear fault symptoms in current signals is indispensable for effective fault diagnosis. Under steady states, mechanical load faults lead to periodic torque oscillations, Blödt *et al.* [16] considered such effects on induction motor currents, and derived a phase modulation (PM) model after certain simplifications. Considering torque oscillations due to gear faults, Kia *et al*. [17], [18] modeled induction motor currents as PM processes for fixed shaft gearbox fault diagnosis, and they extracted gear fault features from Fourier spectrum and phase demodulated spectrum. (Note: PM shares the same modulation nature as frequency modulation (FM), we use FM hereafter.) These works provide useful references for motor current modeling in gear fault cases. However, they focus on fixed shaft gearboxes only, while planetary gearboxes have far more complex kinematics than fixed shaft ones. Even for a single stage, multiple sun–planet and planet–ring gear pairs are in meshing simultaneously. Moreover, gear faults do not lead to FM phenomenon only, but also AM effect (to be explained in Section II). That is why gear fault frequency can be traced via amplitude demodulation in [19], but wherein the AM effect has not been investigated and explained. A simplified FM model is inadequate to fully reveal the gear fault characteristics in the current signals, and confines feature extraction to frequency demodulation only. Therefore, in-depth investigation into the modulation characteristics of current signals under planetary gearbox faults are necessary.

In this paper, in addition to gear fault FM phenomena, we also incorporate gear fault AM effects which are omitted under stringent assumptions in reported works, and model motor current signals as AM-FM processes. Such a comprehensive model will address the limitations imposed by the simplified FM model, give an insight into the gear fault modulation effect on motor currents, and inspire both amplitude and frequency demodulation analyses. As a result, planetary gearbox fault features will be revealed in more details and explained more reasonably. Hereafter, this paper is organized as follows. In Section II, gear fault amplitude and PM effects on motor currents are explained explicitly through mechanical—magnetic–electric interaction analysis, and an AM-FM model is derived. Meanwhile, gear fault features in sidebands and amplitude and frequency demodulation spectra are summarized explicitly, and corresponding fault feature extraction methods are proposed. In Section III, lab experimental signals are analyzed to validate theoretical derivations. In Section IV, conclusions are drawn. This paper involves signature extraction from a large amount of current signals collected at high sampling frequency, and, therefore, closely relates to big data analysis.

II. AM-FM Current Signal Model

A. Stator Current Signal Model

Planetary gearboxes are usually integrated with induction machines to work as a drivetrain. In this paper, we focus on the induction motor case for example.

Under steady states, gear faults or imperfections generate periodic torque oscillations at gear characteristic frequencies. For the sake of clarity and simplicity, we consider only the fundamental gear fault frequency ω_g, then the load torque of induction motor can be formulated as

$$T_l(t) = \bar{T} + T_g \sin(\omega_g t + \varphi_g) \tag{1}$$

where $\bar{T}$ denotes the average load torque, the second term indicates torque oscillation due to gear fault, T_g represents the torque oscillation amplitude, and φ_g is an initial phase.

Under steady states, the induction motor torque T_m equals the average load torque $\bar{T}$, then the rotor speed

$$\omega_r(t) = \frac{1}{J}\int_0^t [T_m - T_l(\tau)]\mathrm{d}\tau = \bar{\omega}_r + \frac{T_g}{J\omega_g}\cos(\omega_g t + \varphi_g) \tag{2}$$

where J is the total rotary inertia of rotating parts, and $\bar{\omega}_r$ is the average motor rotor speed.

The rotor angular position $\theta_r(t)$ can be derived by integrating the motor rotor speed $\omega_r(t)$

$$\theta_r(t) = \int_0^t \omega_r(\tau)\mathrm{d}\tau = \bar{\omega}_r t + \frac{T_g}{J\omega_g^2}\sin(\omega_g t + \varphi_g). \tag{3}$$

The rotor magnetomotive force is dependent on the rotor angular position $\theta_r(t)$. In rotor reference frame, it is written as

$$F_r(\theta_r^{(r)}, t) = F_r \sin(p\theta_r^{(r)} - s\omega_{ps} t) \tag{4}$$

where $\theta_r^{(r)}$ is the rotor angle in rotor reference frame, p is the number of pole pairs, ω_{ps} is the power supply frequency, and s is the motor slip. According to the relationship between rotor and stator reference frame $\theta_r^{(r)} = \theta_s - \theta_r(t)$, where θ_s is the rotor angular position in stator reference frame, the relationship between power supply and rotor rotating frequencies $(1-s)\omega_{ps} = p\bar{\omega}_r$, and incorporating equation (3), the rotor magnetomotive force in stator reference frame can be derived as

$$F_r(\theta_s, t) = F_r \sin\left[p\theta_s - \omega_{ps}t - \frac{pT_g}{J\omega_g^2}\sin(\omega_g t + \varphi_g)\right]. \quad (5)$$

The stator magnetomotive force $F_s(\theta_s, t)$ is independent on the gear fault induced torque oscillation, when only the primary armature is considered, and, therefore, can be written in stator reference frame as

$$F_s(\theta_s, t) = F_s \sin(p\theta_s - \omega_{ps}t). \quad (6)$$

The total magnetomotive force $F(\theta_s, t)$ of both stator and rotor in stator reference frame can be expressed as [13]

$$F(\theta_s, t) = F_s(\theta_s, t) + F_r(\theta_s, t) = F_s \sin[p\theta_s - \omega_{ps}t] + F_r \sin\left[p\theta_s - \omega_{ps}t - \frac{pT_g}{J\omega_g^2}\sin(\omega_g t + \varphi_g)\right]. \quad (7)$$

Assume a constant gap permeance Λ, the air-gap flux density is

$$B(\theta_s, t) = \Lambda F(\theta_s, t) = B_s \sin[p\theta_s - \omega_{ps}t] + B_r \sin\left[p\theta_s - \omega_{ps}t - \frac{pT_g}{J\omega_g^2}\sin(\omega_g t + \varphi_g)\right]. \quad (8)$$

The air-gap flux can be derived by integrating equation (8) over the angle in stator reference frame θ_s (i.e., the winding structure). The winding structure affects the flux harmonic amplitude only; hence, the air-gap flux in an arbitrary phase has the same frequency structure as the magnetomotive force

$$\Phi(t) = \Phi_s \sin(\omega_{ps}t) + \Phi_r \sin\left[\omega_{ps}t + \frac{pT_g}{J\omega_g^2}\sin(\omega_g t + \varphi_g)\right]. \quad (9)$$

The stator voltage $V(t)$, stator current $I(t)$ in an arbitrary phase, and flux $\Phi(t)$ satisfy the following relationship:

$$V(t) = R_s I(t) + \dot{\Phi}(t) \quad (10)$$

where R_s is the stator resistance.

Since the stator voltage is imposed by voltage source, the stator current $I(t)$ is linear to the time derivative of flux $\dot{\Phi}(t)$, and can be modeled by (11), where I_s and I_r are the magnitude of stator resistive current and stator active current, respectively. The first term is a pure sinusoidal component, while the second term features both AM and FM. In summary, (11) implies that gear faults or imperfections have both FM and AM effect on stator current signal, with the carrier frequency equal to the power supply frequency and the FM and AM modulating frequencies equal to gear characteristic frequencies, such as gear fault, rotating, and meshing frequency

$$I(t) = I_s\omega_{ps}\cos(\omega_{ps}t) - I_r \underbrace{\left[\omega_{ps} + \frac{pT_g}{J\omega_g}\cos(\omega_g t + \varphi_g)\right]}_{\text{AM by gear fault}} \times \cos\left[\omega_{ps}t + \underbrace{\frac{pT_g}{J\omega_g^2}\sin(\omega_g t + \varphi_g)}_{\text{FM by gear fault}}\right]. \quad (11)$$

For the current signal model, (11), if the second term in the AM part is neglected, the model becomes a sinusoidal wave plus a pure FM component, which has been investigated in [16]–[18]. However, the conditions for this hold true are stringent. It requires $pT_g/(J\omega_g) \approx 0$, which is not usually the case. In our proposed model, (11), the second term in the AM part is not neglected. As such, the model is generalized to accommodate a more general case. More importantly, it motivates both amplitude and frequency demodulation analyses for gear fault feature extraction.

B. Fourier Spectrum

According to Jacobi–Anger expansion

$$\exp[jz\sin(\theta)] = \sum_{m=-\infty}^{\infty} J_m(z)\exp(jm\theta) \quad (12)$$

where $J_k(z)$ is a Bessel function of the first kind with integer order k and argument z, and the identities of trigonometric functions, (11) can be rewritten as

$$\begin{aligned} I(t) &= I_s\omega_{ps}\cos(\omega_{ps}t) - I_r\left[\omega_{ps} + \frac{pT_g}{J\omega_g}\cos(\omega_g t + \varphi_g)\right] \\ &\quad \times \sum_{k=-\infty}^{\infty} J_k\left(\frac{pT_g}{J\omega_g^2}\right)\cos\{[\omega_{ps} + k\omega_g]t + k\varphi_g\} \\ &= I_s\omega_{ps}\cos(\omega_{ps}t) - I_r\omega_{ps}\sum_{k=-\infty}^{\infty} J_k\left(\frac{pT_g}{J\omega_g^2}\right) \\ &\quad \times \cos\{[\omega_{ps} + k\omega_g]t + k\varphi_g\} - \frac{I_r pT_g}{2J\omega_g}\sum_{k=-\infty}^{\infty} J_k\left(\frac{pT_g}{J\omega_g^2}\right) \\ &\quad \times (\cos\{[\omega_{ps} + (k+1)\omega_g]t + (k+1)\varphi_g\} \\ &\quad + \cos\{[\omega_{ps} + (k-1)\omega_g]t + (k-1)\varphi_g\}). \end{aligned} \quad (13)$$

Applying Fourier transform to (13), yields the Fourier spectrum of stator current, as expressed by (14), where $\delta(\cdot)$ stands for Dirac function. Peaks exist at the power supply frequency ω_{ps}, and the power supply frequency plus or minus the gear fault frequency harmonics $\omega_{ps} \pm k\omega_g$. These peaks form sidebands around the power supply frequency ω_{ps}, with a spacing equal to the gear fault frequency ω_g. Such characteristics can be

explored to detect gear faults

$$I(\omega) = I_s\omega_{ps}\delta(\omega-\omega_{ps}) - I_r\omega_{ps}\sum_{k=-\infty}^{\infty} J_k\left(\frac{pT_g}{J\omega_g^2}\right) \times \delta[\omega-(\omega_{ps}+k\omega_g)]\exp(jk\varphi_g) - \frac{I_r pT_g}{2J\omega_g}\sum_{k=-\infty}^{\infty} J_k \times \left(\frac{pT_g}{J\omega_g^2}\right)(\delta\{\omega-[\omega_{ps}+(k+1)\omega_g]\}\exp[j(k+1)\varphi_g] + \delta\{\omega-[\omega_{ps}+(k-1)\omega_g]\}\exp[j(k-1)\varphi_g]). \quad (14)$$

Although the spacing between neighboring sideband peaks is regular, the sideband magnitudes are not symmetric about the carrier frequency, i.e., power supply frequency ω_{ps}. At any frequency $\omega_{ps}+k\omega_g$, the sideband magnitude

$$I(\omega_{ps}+k\omega_g) = I_r\omega_{ps}J_k\left(\frac{pT_g}{J\omega_g^2}\right)\exp(jk\varphi_g) - \frac{I_r pT_g}{2J\omega_g}J_{k+1}\left(\frac{pT_g}{J\omega_g^2}\right)\exp[j(k+1)\varphi_g] - \frac{I_r pT_g}{2J\omega_g}J_{k-1}\left(\frac{pT_g}{J\omega_g^2}\right)\exp[j(k-1)\varphi_g]. \quad (15)$$

According to the property of Bessel functions

$$J_{-k}(z) = (-1)^k J_k(z) \quad (16)$$

at the counterpart frequency $\omega_{ps}-k\omega_g$, the sideband magnitude

$$I(\omega_{ps}-k\omega_g) = I_r\omega_{ps}(-1)^k J_k\left(\frac{pT_g}{J\omega_g^2}\right)\exp(-jk\varphi_g) - \frac{I_r pT_g}{2J\omega_g}(-1)^k J_{k+1}\left(\frac{pT_g}{J\omega_g^2}\right)\exp[-j(k+1)\varphi_g] - \frac{I_r pT_g}{2J\omega_g}(-1)^k J_{k-1}\left(\frac{pT_g}{J\omega_g^2}\right)\exp[-j(k-1)\varphi_g]. \quad (17)$$

According to (15) through (17), the sidebands are asymmetrical about the power supply frequency ω_{ps}. This is a unique property characteristic of AM-FM signal, and makes AM-FM signal far different from AM and FM signals, which have sidebands symmetrical about the signal carrier frequency.

Fourier spectrum involves intricate sidebands, and sideband peaks do not equal gear fault frequencies directly, thus resulting in difficulty in effective fault diagnosis. Therefore, advanced analysis is necessary to extract fault features more straightforwardly.

C. Amplitude Demodulated Spectrum

To overcome the difficulty due to intricate sidebands in Fourier spectrum, the AM feature can be exploited. For the signal model, (11), the AM-FM term is concentrated since it contains gear fault information, and its AM part

$$a(t) = I_r\left[\omega_{ps}+\frac{pT_g}{J\omega_g}\cos(\omega_g t+\varphi_g)\right]. \quad (18)$$

Its modulating frequency equals the gear fault frequency ω_g. As such, gear fault can be detected through an amplitude demodulation analysis.

Applying Fourier transform to (18), yields the envelope spectrum

$$A(\omega) = I_r[\omega_{ps}\delta(\omega)+\frac{pT_g}{J\omega_g}\delta(\omega-\omega_g)\exp(j\varphi_g)]. \quad (19)$$

Equation (19) shows the existence of gear fault frequency ω_g in the envelope spectrum. If we consider higher harmonics of AM modulating frequency in the signal model, (11), the gear fault frequency harmonics $k\omega_g$ will also emerge in the envelope spectrum. The envelope spectrum is free from intricate sidebands existent in Fourier spectrum, and the present peaks link to the gear fault frequency or its harmonics directly, thus making an envelope spectrum more effective to extract gear fault features. According to such characteristics, gear faults can be detected through an amplitude demodulation analysis.

D. Frequency Demodulated Spectrum

The FM feature can also be exploited to avoid the difficulty due to intricate sidebands in Fourier spectrum, since the FM modulating frequency amounts the gear fault frequency ω_g.

For the signal model, (11), the AM-FM term is concentrated since it contains gear fault information, and its instantaneous phase

$$\alpha(t) = \omega_{ps}t+\frac{pT_g}{J\omega_g^2}\sin(\omega_g t+\varphi_g). \quad (20)$$

Its instantaneous frequency (IF) is a derivative of the instantaneous phase $\alpha(t)$ with respect to time t

$$\omega(t) = \frac{d\alpha(t)}{dt} = \omega_{ps}+\frac{pT_g}{J\omega_g}\cos(\omega_g t+\varphi_g). \quad (21)$$

Applying Fourier transform to (21), yields the Fourier spectrum of IF

$$\Omega(\omega) = \omega_{ps}\delta(\omega)+\frac{pT_g}{J\omega_g}\delta(\omega-\omega_g)\exp(j\varphi_g). \quad (22)$$

Equation (22) implies peak appearance at the gear fault frequency ω_g in the Fourier spectrum of IF. If we consider higher harmonics of the FM modulating frequency in the signal model, peaks will also appear at the gear fault frequency harmonics $k\omega_g$. Based on such features, gear faults can be detected according to the frequency locations of peaks present in the Fourier spectrum of IF.

E. Analysis Procedure

Based on the above theoretical derivations, we propose to extract planetary gearbox fault features from Fourier spectrum, and amplitude and frequency demodulated spectra (see Fig. 1).

First, we analyze the sideband feature around the power supply frequency in the Fourier spectrum of raw signal.

Second, we decompose the raw signal into monocomponents and select the sensitive monocomponent for further demodulation analysis: 1) Decompose the raw signal into intrinsic-mode functions (IMFs) to meet monocomponent requirement by IF

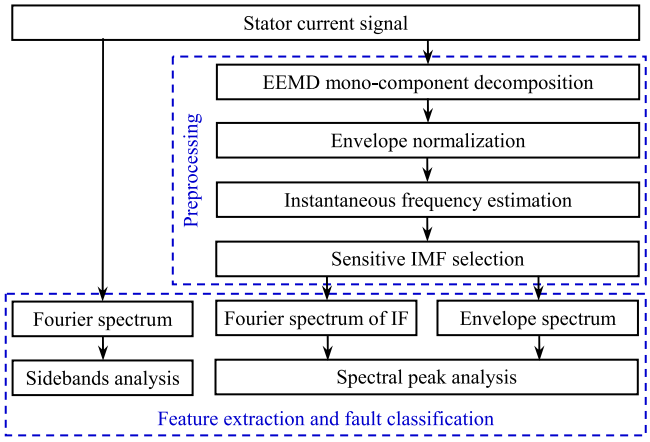

Fig. 1. Analysis flowchart.

estimation, through ensemble empirical-mode decomposition (EEMD) by exploiting its capability to decompose multicomponent signal into constituent monocomponents and robustness to noise interferences [20], [21]. 2) Envelope normalize IMFs to remove the AM effect on IF estimation, thus meeting the requirement by Bedrosian and Nuttall theorem, i.e., nonoverlap between the spectra of carrier signal and amplitude envelope [22], [23]. 3) Estimate the IF of each IMF via Hilbert-transform-based analytic signal approach. 4) Among the IMFs, choose the IMF with an IF fluctuating around the power supply frequency as the sensitive monocomponent, because gear fault modulation is carried by the power supply frequency.

Then, we resolve the AM modulating frequency from the envelope spectrum of sensitive IMF: 1) Apply Hilbert transform to the sensitive IMF. 2) Construct the analytic signal. 3) Calculate the modulus of analytic signal as the amplitude envelope. 4) Generate envelope spectrum by applying Fourier transform to the amplitude envelope.

Next, we generate frequency demodulated spectrum by applying a Fourier transform to the IF of selected sensitive IMF, and identify the FM modulating frequency via a frequency demodulation analysis.

Finally, we diagnose gear fault by combing the findings from sideband analysis in Fourier spectrum, and amplitude and frequency demodulation analyses.

III. Experimental Validation

A. Test Settings

Experiments are conducted on an induction motor-planetary gearbox-magnetic powder brake system to validate the theoretical derivations. Fig. 2 shows the test rig, and Fig. 3 illustrates the planetary gearbox schematic.

An NGW21 planetary gearbox is driven through the input shaft (connected to the sun gear) by a 4-kW SNMA YP-50-4-4 three-phase induction motor with two pole pairs. A 55-lb-in load is applied to the output shaft (connected to the planet carrier) by a CZ-5 magnetic powder brake. The induction motor is controlled by an ABB ACS550 variable frequency drive, stator current signals are measured by Fluke 80i-110s ac/dc current clamps

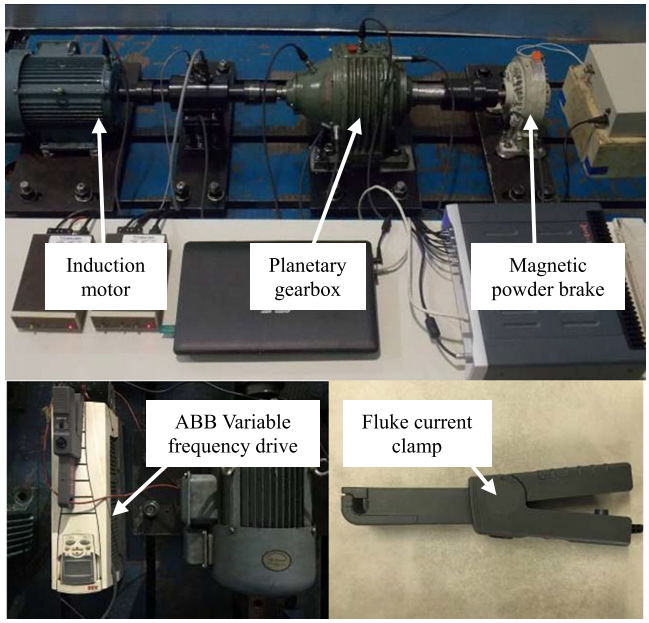

Fig. 2. Planetary gearbox test rig.

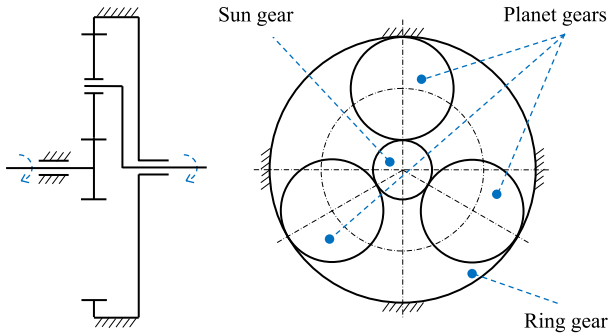

Fig. 3. Planetary gearbox schematic.

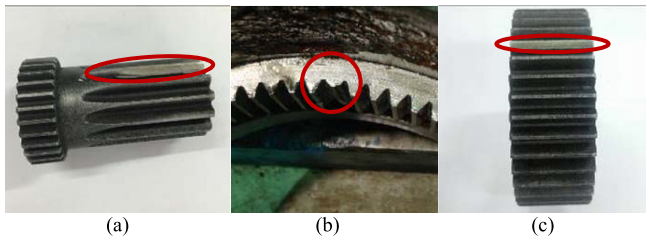

Fig. 4. Localized gear faults: (a) Sun gear, (b) ring gear, and (c) planet gear.

(with an effective bandwidth 0, 20 kHz) between the induction motor and the variable frequency drive, and are collected at 20 kHz.

Four groups of tests are carried out: baseline case when all gears are fault free, faulty sun, planet, and ring gear case when one tooth of the sun gear, one of planet gears, and the ring gear alone is locally chipped, respectively, as shown in Fig. 4(a)–(c).

In all experiments, the power supply frequency is set as 46.8 Hz, thus the induction motor speed equal to 23.4 Hz. Given

TABLE I
PLANETARY GEARBOX CONFIGURATION AND CHARACTERISTIC FREQUENCIES (NOTE: NUMBER OF PLANETS IN PARENTHESIS)

	Motor	Sun	Planet	Ring	Carrier
Number of gear tooth	-	13	38 (3)	92	-
Running frequency (Hz)	f_{ps}=46.8	$f_s^{(r)} = 23.4$	$f_p^{(r)} = 4.1$	-	$f_c = 2.9$
Localized fault frequency (Hz)	-	$f_s = 61.5$	$f_{p1} = 7, f_{p2} = 14$	$f_r = 8.7$	-

gear configurations listed in Table I, the gearbox characteristic frequencies are calculated (see Table I).

B. Signal Analysis

Fig. 5 shows the baseline signal analysis result. Note: Hereafter, we denote all the characteristic frequencies with a symbol f in a unit of Hertz. In the Fourier spectrum, Fig. 5(b), the power supply frequency f_{ps} dominates, and its harmonics nf_{ps} also have pronounced magnitude. Meanwhile, some sidebands appear, and they relate to the power supply frequency harmonics plus or minus the sun gear and the planet carrier rotating frequency harmonics, i.e., $nf_{ps} \pm kf_s^{(r)}$ and $nf_{ps} \pm lf_c$, where $n, k, l = 1, 2, \ldots$. In amplitude demodulation analysis, the envelope spectrum, Fig. 5(d), displays prominent peaks at the sun gear and the planet carrier rotating frequency harmonics $kf_s^{(r)}$ and lf_c, as well as their sum or difference combinations $kf_s^{(r)} \pm lf_c$. For frequency demodulation analysis, the raw signal is decomposed into a number of IMFs via EEMD to meet the monocomponent requirement by IF estimation. Then, a sensitive IMF with its IF fluctuating around the power supply frequency is selected for further analysis. Fig. 5(g) presents the Fourier spectrum of sensitive IMF IF. Dominant peaks correspond to the sun gear rotating frequency harmonics $kf_s^{(r)}$. Prominent peaks appear at the planet carrier rotating frequency harmonics lf_c, and the sum or difference combinations of sun gear and planet carrier rotating frequency harmonics $kf_s^{(r)} \pm lf_c$. The presence of these frequency harmonics and their combinations in Fourier spectrum, or amplitude and frequency demodulated spectra are reasonable, because gearbox manufacturing errors are inevitable. These imperfections lead to load torque oscillation, and result in AM-FM effect at those rotating frequencies. However, prominent peaks do not show up at any gear fault frequency in Fourier spectrum, or amplitude and frequency demodulated spectra. This implies nonexistence of gear fault, consistent with the fault free setting in the baseline case.

Fig. 6 demonstrates the sun fault signal analysis results. Those frequencies present in the baseline signal still exist in the Fourier spectrum, and the amplitude and frequency demodulated spectra. However, pronounced peaks appear at the sun gear fault frequency plus and minus the power supply frequency $f_s \pm f_{ps}$, as marked by dot in the Fourier spectrum [see Fig. 6(a)]. In both amplitude demodulated spectrum of raw signal and frequency demodulated spectrum of sensitive IMF, Fig. 6(b) and (c), prominent peaks emerge at the sun gear fault frequency f_s and its twice $2f_s$. These findings indicate fault existence on the sun gear.

Fig. 7 illustrates the planet gear fault signal analysis results. In the Fourier spectrum, Fig. 7(a), some new peaks show up at sum and difference combination of the power supply frequency, sun gear, planet gear, and planet carrier rotating frequency harmonics, i.e., $f_{ps} \pm kf_s^{(r)} \pm lf_c \pm mf_p^{(r)}$. More importantly, prominent peaks emerge at the power supply frequency plus and minus twice the planet gear fault frequency $f_{ps} \pm 2f_{p1}$. In the amplitude and frequency demodulated spectra, Fig. 7(b) and (c), new peaks emerge at the planet gear fault frequency harmonics nf_{p1}. These features imply fault occurrence on one planet gear.

Fig. 8 presents the ring gear fault signal analysis results. In the Fourier spectrum, Fig. 8(a), sidebands related to the ring gear fault frequency, $f_{ps} \pm f_r$, are discovered. New peaks appear at the power supply frequency plus or minus sum and difference combination of the sun gear, planet gear, and planet carrier rotating frequency harmonics, i.e., $f_{ps} \pm kf_s^{(r)} \pm lf_c$ and $f_{ps} \pm kf_s^{(r)} \pm lf_c \pm mf_p^{(r)}$. In the envelope spectrum, Fig. 8(b), the ring gear fault frequency harmonics f_r, $2f_r$, and $3f_r$ show nonnegligible magnitude, in addition to the peaks at sum and difference combination of the sun gear, planet gear, and planet carrier rotating frequency harmonics $kf_s^{(r)} \pm lf_c \pm mf_p^{(r)}$. In the Fourier spectrum of sensitive IMF IF, Fig 8(c), a nonnegligible peak emerges at the ring gear fault frequency f_r. Meanwhile, prominent peaks exist at sum and difference combination of the sun gear, planet gear, and planet carrier rotating frequency harmonics $kf_s^{(r)} \pm lf_c \pm mf_p^{(r)}$. In both Fourier spectrum, amplitude and frequency demodulated spectra, more peaks emerge and relate to planet carrier rotating frequency f_c. Because of inevitable minor difference between planet gears due to manufacturing imperfection, ring gear fault impulses differ among all the three planet gears as they contact the faulty ring gear tooth. In this case, ring gear faults are characterized by a separate impulse train that is generated as the faulty ring gear tooth meshes with one of the planet gears. As such, the effect of number of planet gears can be omitted, and ring gear fault is manifested by the planet carrier rotating frequency $f_c = f_p/3$. These signatures mean presence of the ring gear fault.

The above experimental signal analyses verify the proposed AM-FM current signal model. In all the four cases, Fourier spectra show an asymmetric frequency structure about the power supply frequency. This complies with the sideband asymmetry of AM-FM signals. Moreover, in the envelope spectra, gear fault frequency harmonics do exist with a nonnegligible magnitude. This again confirms the gear fault AM effect, in addition to the FM effect, on induction motor currents. Most importantly, this insight into the AM-FM nature of current signals lays a

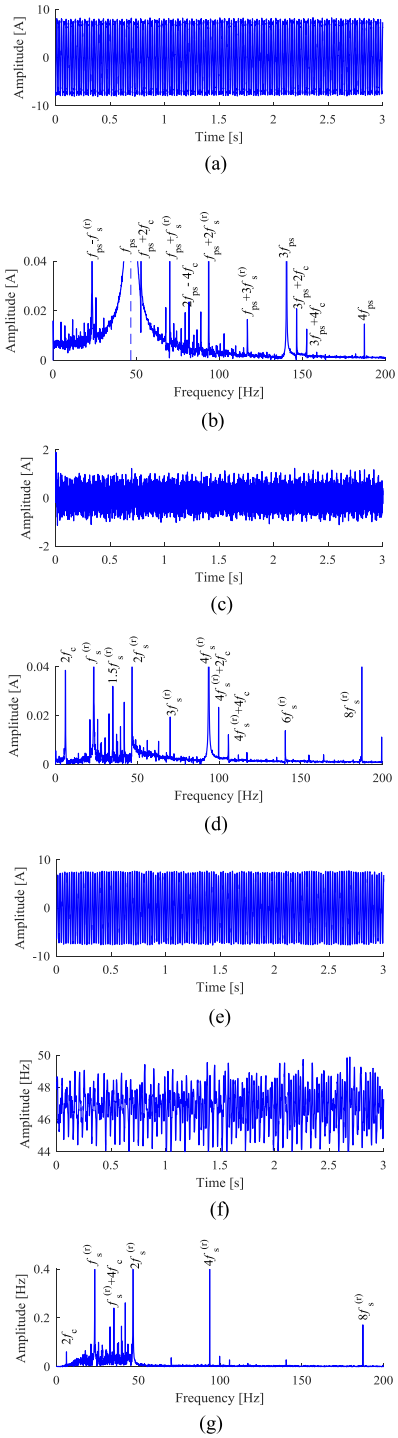

Fig. 5. Baseline signal analysis result: (a) Raw signal waveform, (b) Fourier spectrum of raw signal, (c) detrended amplitude envelope waveform, (d) envelope spectrum, (e) sensitive IMF waveform, (f) IF of sensitive IMF, and (g) Fourier spectrum of sensitive IMF IF.

foundation for planetary gearbox fault feature extraction through amplitude demodulation analysis.

The analysis results also validate the theoretical derivations based on the proposed AM-FM signal model. In Fourier spectra, sidebands correspond to the power supply frequency plus or minus the gearbox characteristic frequency harmonics. In

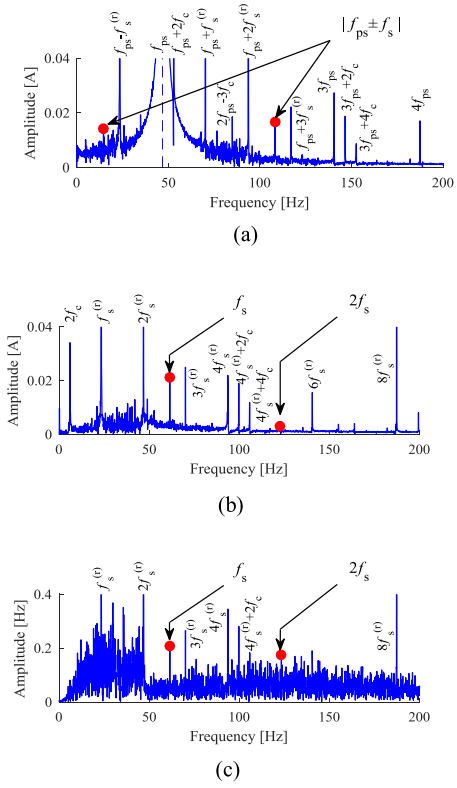

Fig. 6. Sun gear fault signal analysis result: (a) Fourier spectrum of raw signal, (b) envelope spectrum, and (c) Fourier spectrum of sensitive IMF IF.

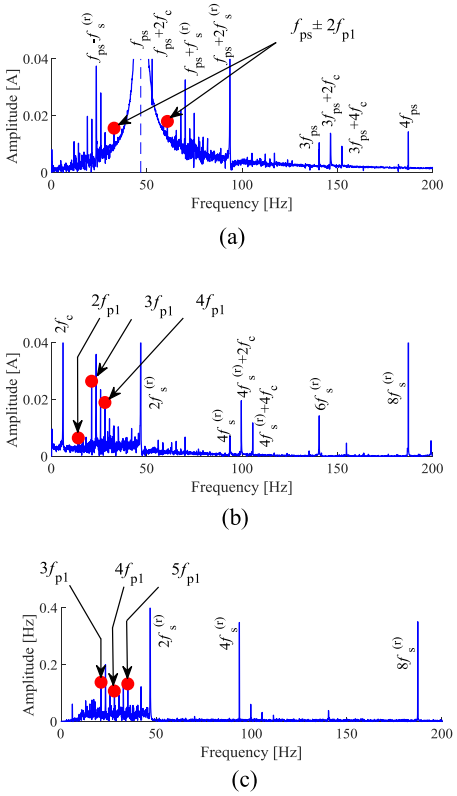

Fig. 7. Planet gear fault signal analysis result: (a) Fourier spectrum of raw signal, (b) envelope spectrum, and (c) Fourier spectrum of sensitive IMF IF.

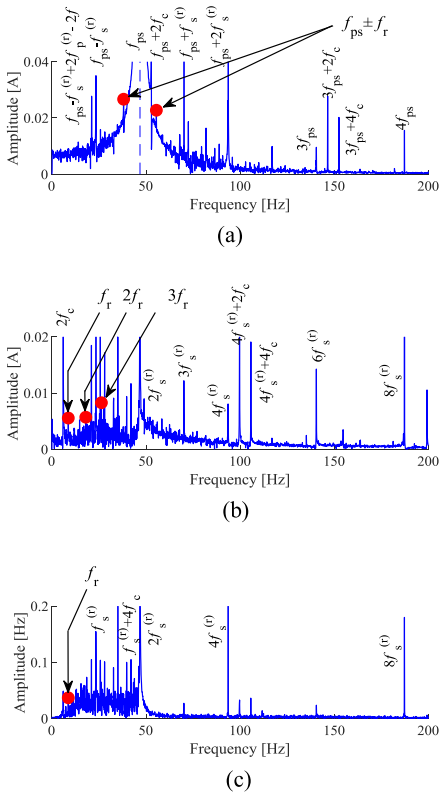

Fig. 8. Ring gear fault signal analysis result: (a) Fourier spectrum of raw signal, (b) envelope spectrum, and (c) Fourier spectrum of sensitive IMF IF.

amplitude and frequency demodulated spectra, peaks link to the gearbox characteristic frequency harmonics. These characteristics are consistent with the theoretical derivations. More importantly, the findings are in accordance with the actual experimental setting.

This paper focuses on gear fault diagnosis through detecting the presence or magnitude change of gear fault frequency. Electric factors irrelevant to gear faults are omitted in the developed signal model, such as parametric variations in induction motor, power supply quality, and voltage imbalances, because their frequencies are far different from planetary gearbox fault frequencies. Moreover, frequencies due to the above inevitable electric factors are present in all the experimental cases. Gear faults are confirmed by comparing the current signature of gear fault frequencies in the fault case against that in the baseline case. This helps us to improve the robustness of the proposed methodology to electric factors.

IV. Conclusion

Gear faults generate load torque oscillations, leading to both AM and FM effects on induction motor current signals. Based on a mechanical—magnetic–electric interaction analysis, an AM-FM signal model is proposed to better characterize induction motor stator currents in planetary gearbox fault cases under constant running conditions, wherein the carrier frequency amounts the power supply frequency, and the AM and FM modulating frequencies equal the gear fault frequency. Explicit equation of its Fourier spectrum is derived. Asymmetric sidebands exist around the power supply frequency with a spacing equal to the gear fault frequency. An insight into the AM-FM nature of current signals inspires both amplitude and frequency demodulation analysis to overcome the difficulty due to intricate sidebands, by exploiting the fact that the AM and FM modulating frequencies relate to the gear fault frequency. According to derived explicit equations, the gear fault frequency harmonics dominate the amplitude and frequency demodulated spectra. The theoretical derivations are validated through experimental signal analysis of an induction motor–planetary gearbox electromechanical system. Localized faults on all the three types of gear (sun, planet, and ring) are successfully diagnosed. Both the developed signal model and the proposed analysis method can be generalized to fixed-shaft gearbox fault diagnosis.

Acknowledgment

The authors would like to thank anonymous reviewers and the Editor for their comments.

References

[1] S. T. Kandukuri, A. Klausen, H. R. Karimi, and K. G. Robbersmyr, "A review of diagnostics and prognostics of low-speed machinery towards wind turbine farm-level health management," *Renew. Sustain. Energy Rev.*, vol. 53, pp. 697–708, Jan. 2016.

[2] Y. Lei, J. Lin, M. J. Zuo, and Z. He, "Condition monitoring and fault diagnosis of planetary gearboxes: A review," *Measurement*, vol. 48, pp. 292–305, Feb. 2014.

[3] X. Liang, M. J. Zuo, and Z. Feng, "Dynamic modeling of gearbox faults: A review," *Mech. Syst. Signal Process.*, vol. 98, pp. 852–876, Jan. 2018.

[4] W. Bartelmus, F. Chaari, R. Zimroz, and M. Haddar, "Modelling of gearbox dynamics under time-varying nonstationary load for distributed fault detection and diagnosis," *Eur. J. Mech. A/Solids*, vol. 29, pp. 637–646, Mar. 2010.

[5] A. Hammami, A. Rincon, F. Chaari, M. Santamaria, F. Rueda, and M. Haddar, "Effects of variable loading conditions on the dynamic behavior of planetary gear with power recirculation," *Measurement*, vol. 94, pp. 306–315, Dec. 2016.

[6] Y. Lei, D. Han, J. Lin, and Z. He, "Planetary gearbox fault diagnosis using an adaptive stochastic resonance method," *Mech. Syst. Signal Process.*, vol. 38, pp. 113–124, Jul. 2013.

[7] J. Yoon, D. He, B. V. Hecke, T. J. Nostrand, J. D. Zhu, and E. Bechhoefer, "Vibration-based wind turbine planetary gearbox fault diagnosis using spectral averaging," *Wind Energy*, vol. 19, no. 9, pp. 1733–1747, Sep. 2016.

[8] Z. Feng and M. J. Zuo, "Vibration signal models for fault diagnosis of planetary gearboxes," *J. Sound Vibr.*, vol. 331, pp. 4919–4939, Oct. 2012.

[9] Z. Feng, M. Liang, Y. Zhang, and S. Hou, "Fault diagnosis for wind turbine planetary gearboxes via demodulation analysis based on ensemble empirical mode decomposition and energy separation," *Renew. Energy*, vol. 47, pp. 112–126, Nov. 2012.

[10] S. Singh and N. Kumar, "Detection of bearing faults in mechanical systems using stator current monitoring," *IEEE Trans. Ind. Informat.*, vol. 13, no. 3, pp. 1341–1349, Jun. 2017.

[11] R. H. Cunha Palacios, I. N. da Silva, A. Goedtel, W. F. Godoy, and T. D. Lopes, "Diagnosis of stator faults severity in induction motors using two intelligent approaches," *IEEE Trans. Ind. Informat.*, vol. 13, no. 4, pp. 1681–1691, Aug. 2017.

[12] S. S. Lin, Z. G. Liu, and K. T. Hu, "Traction inverter open switch fault diagnosis based on Choi-Williams distribution spectral kurtosis and wavelet-packet energy Shannon entropy," *Entropy*, vol. 19, no. 9, pp. 1–19, Sep. 2017.

[13] A. Glowacz *et al.*, "Fault diagnosis of three phase induction motor using current signal, MSAF-RATIO15 and selected classifiers," *Arch. Metall. Mater.*, vol. 62, no. 4, pp. 2413–2419, Dec. 2017.

[14] J. Zhang, J. S. Dhupia, and C. J. Gajanayake, "Stator current analysis from electrical machines using resonance residual technique to detect faults in planetary gearboxes," *IEEE Trans. Ind. Electron.*, vol. 62, no. 9, pp. 5709–5721, Sep. 2015.

[15] J. R. Ottewill, A. Ruszczyk, and D. Broda, "Monitoring tooth profile faults in epicyclic gearboxes using synchronously averaged motor currents: Mathematical modeling and experimental validation," *Mech. Syst. Signal Process.*, vol. 84, pp. 78–99, Feb. 2017.
[16] M. Blödt, M. Chabert, J. Regnier, and J. Faucher, "Mechanical load fault detection in induction motors by stator current time-frequency analysis," *IEEE Trans. Ind. Appl.*, vol. 42, no. 6, pp. 1454–1463, Nov./Dec. 2006.
[17] S. Kia, H. Henao, and G.-A. Capolino, "Analytical and experimental study of gearbox mechanical effect on the induction machine stator current signature," *IEEE Trans. Ind. Appl.*, vol. 45, no. 4, pp. 1405–1415, Jul. 2009.
[18] S. H. Kia, H. Henao, and G.-A. Capolino, "Gear tooth surface damage fault detection using induction machine stator current space vector analysis," *IEEE Trans. Ind. Electron.*, vol. 62, no. 3, pp. 1866–1878, Mar. 2015.
[19] A. R. Mohanty and C. Kar, "Fault detection in a multistage gearbox by demodulation of motor current waveform," *IEEE Trans. Ind. Electron.*, vol. 53, no. 4, pp. 1285–1297, Aug. 2006.
[20] N. E. Huang *et al.*, "The empirical mode decomposition and the Hilbert spectrum for nonlinear and nonstationary time series analysis," *Proc. Roy. Soc. Lond., Ser. A*, vol. 454, pp. 903–995, Mar. 1998.
[21] Z. Wu and N. E. Huang, "Ensemble empirical mode decomposition: A noise-assisted data analysis method," *Adv. Adapt. Data Anal.*, vol. 1, no. 1, pp. 1–41, Jan. 2009.
[22] A. H. Nuttalll and E. Bedrosian, "On the quadrature approximation on the Hilbert transform of modulated signals," *Proc. IEEE*, vol. 54, no. 10, pp. 1458–1459, Oct. 1966.
[23] N. E. Huang *et al.*, "On instantaneous frequency," *Adv. Adapt. Data Anal.*, vol. 1, no. 2, pp. 177–229, Apr. 2009.

Zhipeng Feng (M'15) received the B.Sc. degree in automotive engineering from Jilin University, Changchun, China, in 1997, the M.Sc. degree in mechanical engineering from Kunming University of Science and Technology, Kunming, China, in 2000, and the Ph.D. degree in power machinery engineering from Dalian University of Technology, Dalian, China, in 2003.

From 2003 to 2005, he was a Postdoctoral Fellow with the Department of Precision Instruments and Mechanology, Tsinghua University, China. From 2006 to 2007, he was a Postdoctoral Research Fellow with the Department of Mechanical Engineering, University of Alberta, Canada. He is currently a Professor with the School of Mechanical Engineering, University of Science and Technology Beijing, Beijing, China. His research interests include machinery fault diagnosis, signal processing, artificial intelligence, and mechanical dynamics.

Xiaowang Chen received the B.Sc. degree in automotive engineering and the Ph.D. degree in mechanical engineering from the University of Science and Technology Beijing, Beijing, China, in 2013 and 2018, respectively.

He was a Visiting Scholar with the Department of Mechanical Engineering, University of Alberta, Canada, from 2016 to 2017. He is currently with the University of Science and Technology Beijing. His research interests include machinery fault diagnosis and nonstationary signal processing.

Ming J. Zuo (SM'00) received the B.Sc. degree in agricultural engineering from Shandong Institute of Technology, Zibo, China in 1982, and the M.Sc. and Ph.D. degrees in industrial engineering from Iowa State University, Ames, IA, USA, in 1986 and 1989, respectively.

He is currently a Professor with the Department of Mechanical Engineering, University of Alberta, Edmonton, AB, Canada. He is a Department Editor for the *IISE Transactions*, a Regional Editor for the *International Journal of Strategic Engineering Asset Management*, and the Editorial Board Member of the Reliability Engineering and System Safety, the *Journal of Traffic and Transportation Engineering*, the *International Journal of Quality, Reliability, and Safety Engineering*, and the *International Journal of Performability Engineering*. His research interests include system reliability analysis, maintenance modeling and optimization, signal processing, and fault diagnosis.

Dr. Zuo is a Fellow of the Institute of Industrial and Systems Engineering, the Engineering Institute of Canada, and the Founding Fellow of the International Society of Engineering Asset Management.